



Radiation Shielding Properties of Synthetic Ca-Al₂O₃ Polymer Based Composites

Mufutau A. Salawu^{1*}, Ibrahim K. Ayinla², Sabastine C. Ezike³, Mojeed O. Bello², Usman O. Usman¹, Abdulmojeed O. Yussuf¹, Julius A. Gbolahan¹, Aderemi B. Alabi¹

¹Department of Physics,
University of Ilorin, Ilorin, P.M.B 1515, NIGERIA

²Department of Chemistry/Industrial Chemistry,
University of Ilorin, Ilorin, P.M.B 1515, NIGERIA

³Department of Physics, School of Physical Sciences,
Modibbo Adama University of Technology, Yola, P.M.B 2076, NIGERIA

*Corresponding Author

DOI: <https://doi.org/10.30880/jsmpm.2023.03.01.002>

Received 09 January 2023; Accepted 19 March 2023; Available online 07 May 2023

Abstract: The optical and radiation shielding capabilities of Ca-Al₂O₃ polymer-based composites were explored by combining synthesized aluminum oxide (Al₂O₃) with calcium (Ca) obtained from different shells. The obtained powders were dispersed into polymeric materials in a ratio of 2:1 via the melt-mixing process and then cast in a 10 cm x 10 cm mold with a thickness of 10 mm and allowed to set at ambient temperature. The X-ray transmission through the composite samples was investigated using a well-collimated point source, and a linear attenuation coefficient was estimated. X-ray fluorescence results revealed calcium contents of 32 %, 37 %, and 34 % for snail shells, seashells, and periwinkle shells, respectively. The X-ray diffraction result confirmed the Al₂O₃ polymorphs at approximately 32° and 57° and the aluminum phase at 46°. The X-ray photon transmittance of the composites is quite low at 40 keV to 60 keV and comparatively higher at 100 keV to 200 keV. For Ca-Al₂O₃ polymer-based composites with calcium contents sourced from seashells, periwinkle shells, and snail shells, the maximum linear attenuation coefficients were 1.0 cm⁻¹, 0.79 cm⁻¹, and 0.65 cm⁻¹, respectively. The half-value layer (HVL) and relaxation length of all the samples under investigation decreased abruptly at 40 keV and 60 keV and grew linearly as the energy increased from 100 keV to 200 keV. A Ca-Al₂O₃ polymer-based composite with calcium contents sourced from seashells was found to have higher x-ray attenuating characteristics than other composites.

Keywords: Ca-Al₂O₃, relaxation length, HVL, epoxy, linear attenuation

1. Introduction

Radiation from traditional X-rays is linked to the exposure of radiosensitive organs, necessitating the use of lead as a shield. However, it has been demonstrated that lead (Pb) can conceal essential anatomical structures during imaging and cause abnormalities, prompting repeat radiography [1,2]. The radiosensitive organs in the lower abdomen, particularly the gonads, are exposed to ionizing radiation during pelvic radiography, which is one of the most common and high-dose examinations for children [3–6]. X-ray examinations can be quite beneficial, but they can have hazards. As a result, deciding whether to have an X-ray takes careful deliberation. Patients with various disorders, such as bone fractures, require medical X-rays for safe diagnosis and accurate realignment under visual control.

Strongly ionizing X-ray is frequently utilized for nondestructive testing, medical diagnosis, medical treatment, geological exploration, and security systems. The biological effects of X-rays have long drawn special attention to their dangers. The International Committee on Radiological Protection has recently classified X-rays as carcinogenic [7]. As a result, shielding X-rays to reduce their carcinogenic and genetic impacts, which can cause cell mutations, has become a critical topic in the field of radiation protection. As a result, X-ray shielding is essentially determined by the likelihood of photoelectric and Compton scattering between incident photons and the shielding material.

When incident photons interact with inner-shell electrons in some materials, the absorption coefficient rises dramatically. The matching energy is known as the material's absorption limit or absorption edge. Because of its high Z number, high density, and inexpensive cost, lead is commonly employed as a shielding material because of its greater ability to efficiently shield X-rays compared to other materials. On the other hand, lead-based shielding materials typically have several severe disadvantages, including high toxicity, heavy nature, limited flexibility, and low chemical stability. They also have a blind absorption zone for X-rays with energies between 70 and 90 keV [7]. As a result, novel shielding materials are urgently needed to replace traditional lead-based shielding materials.

In the described work [8–32], radiation shielding materials were traditionally made from glass, rubber, polymer, elastomeric polymer, or vinyl binders with an elastic matrix packed with microscopic lead particles or lead oxide. Other applications for polymer composite materials have been reported [33-34]. Adsorption of catalysts in polyethylene manufacturing, hydrogen peroxide synthesis, as a selective adsorbent for numerous compounds including arsenic and fluoride, and sulfur removal from gas streams were only some of the applications for Al₂O₃ nanoparticles. Due to their hardness, chemical inertness, high melting point, non-volatility, and resistance to oxidation and corrosion, aluminum oxides have also found used in ceramics, refractories, and abrasives [35-36].

Seashells, periwinkle shells, and snail shells were formerly lucrative resources and a variety of enterprises are currently investigating how they might be used to boost profitability as well as sustainability. Construction materials, food supplements, pharmaceuticals, animal feed, plastic production, and other businesses need mined calcium carbonate, but seashells provide a natural alternative. Seashells and snail shells have the most potential for application in poultry nutrition, water purification, toxic waste removal, organic fertilizer, and building.

Periwinkle shells are found in rivers and coastal locations and come in a "V" form with a circular opening that houses small greenish-blue marine snails. The texture is brittle but exceptionally durable [37-38]. In this paper, we study the radiation shielding capabilities of synthetic Ca-Al₂O₃ polymer-based composite materials that are exceptionally low cost and relatively easy to make and characterize, as well as the impact of calcium content on their potential for x-ray attenuating properties.

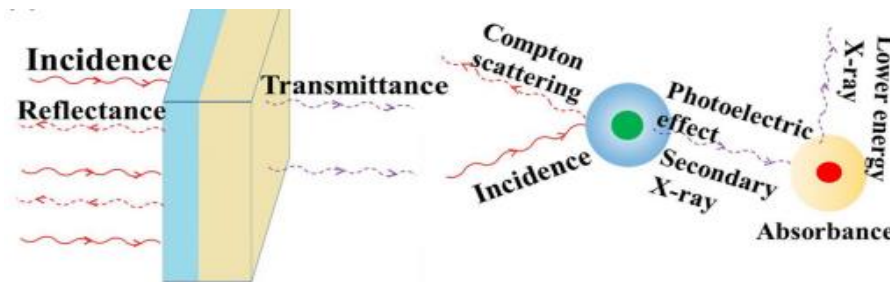


Fig. 1 - Attenuation mechanisms of x-ray [7]

2. Materials and Method

The materials used for this work are the synthesized aluminum oxide powder obtained from Industrial Chemistry Department of University of Ilorin, periwinkle shells, snail shells, and seashells found in Nigeria, aluminum mold, epoxy resin (bisphenol-A-diglycidyl ether poly) and hardener. The instrument used for characterizing the materials are X-ray diffractometer, X-ray fluorescence spectrometer and Radiographic equipment.

2.1 Synthesis of Calcium via Calcination

Calcium (Ca) was synthesized from periwinkle shells, snail shells, and seashells via calcination at 1000 °C for 13 hours. The obtained calcined powdered samples from the shells were characterized using X-ray fluorescence spectrometer to determine the quality and quantity of calcium content and other trace elements present in each of the samples.

2.2 Mixing of Polymer Composites

Melt-mixing procedures in the ratio of 2:1 of epoxy resin (bisphenol-A-diglycidyl ether poly) and hardener (isophoromediamine) was used. The synthesized Ca-Al₂O₃ powders were dispersed into polymeric materials in a ratio of 2:1 using an effective melt-mixing method, then cast in a 10 cm by 10 cm square Mold with a thickness of 10 mm

and allowed to set overnight at ambient temperature. To ensure fairly equal dispersion of the powders in an epoxy matrix, the composites were thoroughly stirred for 20 minutes with a two-roll Rheomixer device at a speed of 60 revolutions per minute (rpm).

2.3 Radiographic Characterizations of the Composites

The composite samples were transferred to the Nigerian Nuclear Regulatory Agency (NNRA) in Ibadan for radiographic examinations and analyses. X-ray transmission through the composites samples was investigated using a well-collimated point source. The produced x-rays' initial intensity (I_0) was determined. With the sample in front of the detector, the transmitted x-ray beam (I) was measured. The measurements were repeated three times for each composite sample, and the average value was determined. Equations 1, 2, and 3 [25] were employed to determine each sample's linear attenuation coefficient, half-value layer, and relaxation length. The radiation shielding composites' x-ray photon absorptions were determined using equation 4 from transmission data by Beer's Lambert law, as published in [39-45].

$$\text{The linear attenuation coefficient } \mu = \frac{\ln \frac{I_0}{I}}{x} \tag{1}$$

$$\text{The Half-Value Layer (HVL)} = \frac{0.693}{\mu} \tag{2}$$

$$\text{Relaxation length } \lambda = \frac{1}{\mu} \tag{3}$$

$$\text{Absorbance } A = 2 - \log_{10} T \tag{4}$$

Where μ is the absorber's linear attenuation (fabricated sample), x is the sample's thickness, I and I_0 are the transmitted and incident x-ray beams, and T is transmittance. The produced Ca-Al₂O₃ polymer-based radiation shielding composites for varied synthesized calcium content levels from different shells are shown in Fig. 2. Fig. 3 depicts the images of periwinkle shells, snail shells, and seashells.



Fig. 2 - Ca-Al₂O₃ polymer-based radiation shielding composites (a) Ca from snail shells; (b) Ca from periwinkle shells, and; (c) Ca from seashells

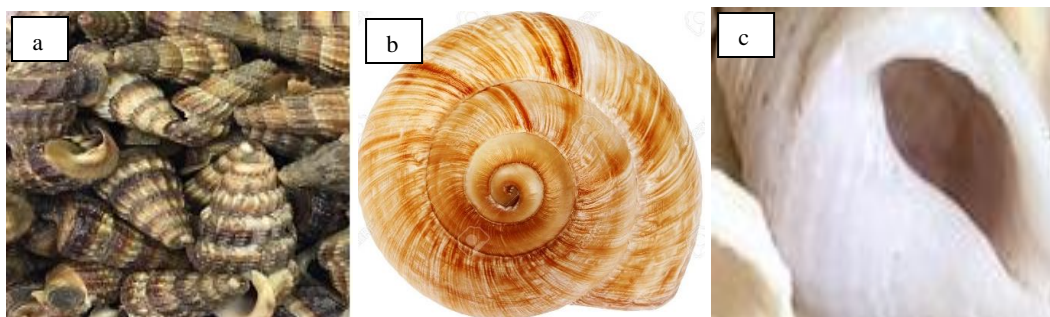


Fig. 3 - Different shells used (a) periwinkle shells; (b) snail shell, and; (c) seashell

3. Results and Discussion

3.1 Synthesized Al₂O₃ Powder X-Ray Diffraction (XRD) Analysis

The XRD analysis of the synthesized Al₂O₃ powder revealed the existence of the aluminum oxide nanoparticle crystal phase and small residues of elemental aluminum. The Al₂O₃ polymorphs were found in the synthesized sample at the sample's peaks of 32° and 57°, respectively, while the aluminum phase was found at about 46°. This observation is consistent with the findings of [36] and is supported by card file No. 46-1215 of the Joint Committee on Powder Diffraction Standards (JCPDS).

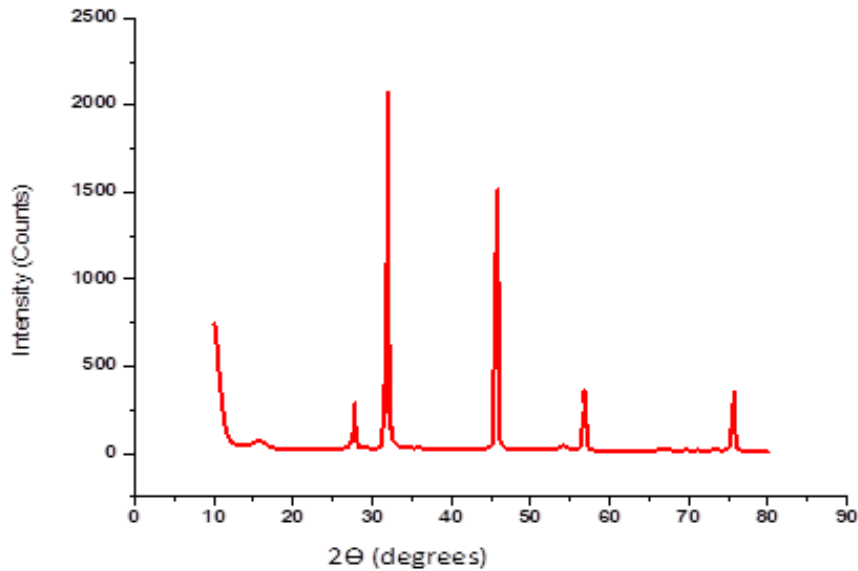


Fig. 4 - X-ray diffraction of the synthesized Al₂O₃ Powder

3.2 X-ray Fluorescence of Calcined Shell Particle Samples

The elemental contents of the calcined samples from the shell particles were determined using an X-ray fluorescence (XRF) analytical method. By detecting the fluorescence (or secondary) X-ray released by a sample when it is excited by the main X-ray source, XRF analyzers determine the chemistry of a sample. Each element in a sample creates a distinct set of fluorescent X-rays ("a fingerprint") that is unique to that element. Table 1 and Fig. 5 exhibits the qualitative and quantitative assessments of synthesized components from each of the shell particles employed.

Phosphorus, Sulphur, Manganese, Iron, Nickel, Copper, Zinc, Molybdenum, Cadmium, Tin, and Antimony contaminants were detected at very small levels in the calcined samples. Snail shells, Seashells, and Periwinkle shells had calcium compositions of 32%, 37%, and 34%, respectively. The results are shown in Table 1 and Fig. 5, respectively.

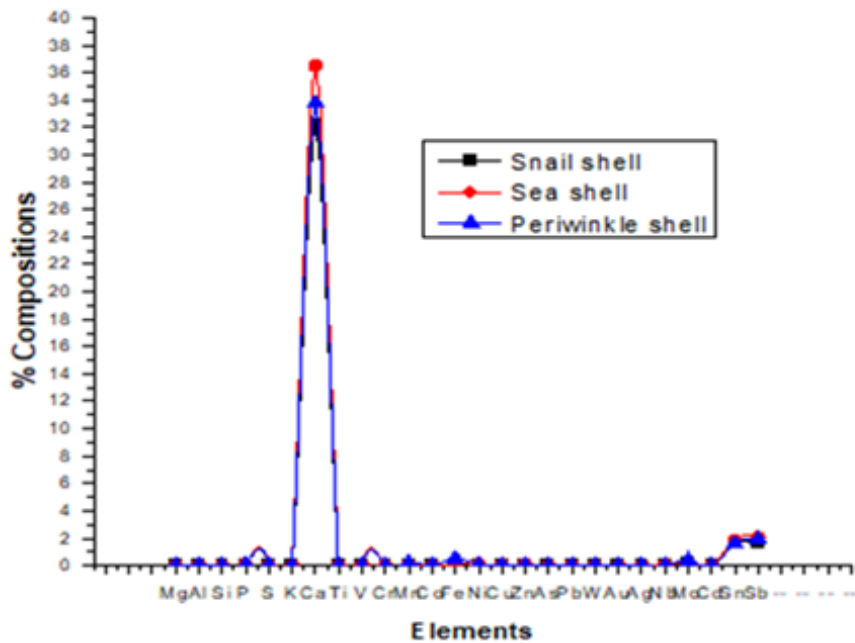


Fig. 5 - XRF analyses of the calcined samples from different shells particles

Table 1 - XRF of the calcined samples from the shell's particles

Element	Snail shell	Seashell	Periwinkle shell
Mg	0.0000	0.0000	0.0000
Al	0.0000	0.0000	0.0000
Si	0.0000	0.0000	0.0000
P	0.0636	0.0822	0.0706
S	0.0202	0.0000	0.0451
K	0.0000	0.0000	0.0000
Ca	32.2261	36.5035	33.7753
Ti	0.0000	0.0000	0.0000
V	0.0000	0.0000	0.0000
Cr	0.0000	0.0000	0.0000
Mn	0.0000	0.0000	0.1857
Co	0.0000	0.0000	0.0000
Fe	0.0850	0.1199	0.5285
Ni	0.0470	0.0540	0.0512
Cu	0.0334	0.0442	0.0214
Zn	0.0737	0.0793	0.0683
As	0.0000	0.0000	0.0000
Pb	0.0000	0.0000	0.0000
W	0.0000	0.0000	0.0000
Au	0.0000	0.0000	0.0000
Ag	0.0000	0.0000	0.0009
Nb	0.0000	0.0167	0.0046
Mo	0.2073	0.1595	0.3720
Cd	0.0000	0.0007	0.0000
Sn	1.5761	1.8693	1.5971
Sb	1.6413	2.0607	1.8887

3.3 Fourier Transform Infrared Spectroscopy (FTIR) Analysis

FTIR spectra of calcined samples from shell particles recorded in the region of 500 to 4000 cm^{-1} are displayed in Fig. 6. For the three calcined samples produced, the C–H bending occurred at around 1465 cm^{-1} , confirming the presence of alkane, while the O–H stretching band at 3700 cm^{-1} suggested the existence of alcohol.

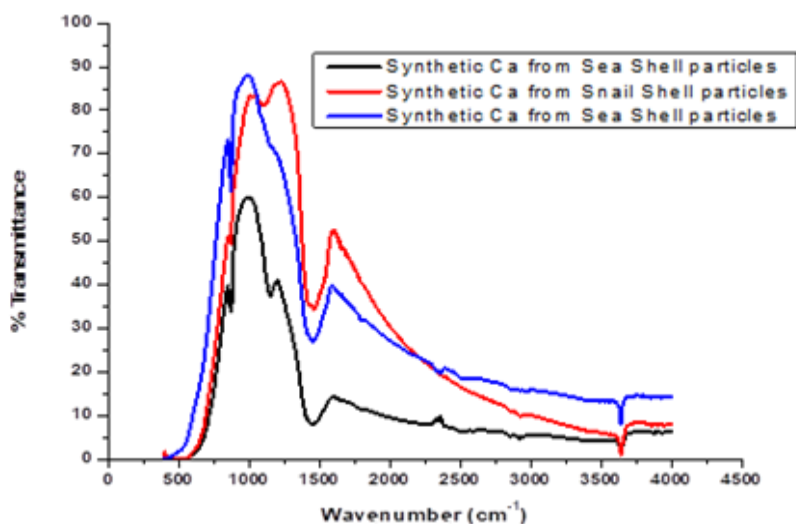


Fig. 6 - FTIR analyses of the calcined samples produced from shell's particles

3.4 Optical Properties of the Produced Radiation Shielding Composites

Transmittance is the number of x-rays that are transmitted to the incident x-rays. The transmittance of x-ray photons changes with the energy of the x-ray and the radiation shielding characteristics of each composite under investigation are shown in Fig. 7. For the three radiation shielding composites, the x-ray photon transmittance is relatively low for energies between 40 and 60 keV and relatively high for energies between 100 and 200 keV. Each radiation shielding composite's properties are determined by the amount of calcium present in the sample. The least transmittance values were found in Ca-Al₂O₃ polymer-based composite with significant calcium content and derived from seashells at the various energies studied. From 100 keV to 200 keV, the transmittance of Periwinkle shells and Snail shell calcium sources was similar, but the difference became significant at relatively low energies between 40 keV and 60 keV.

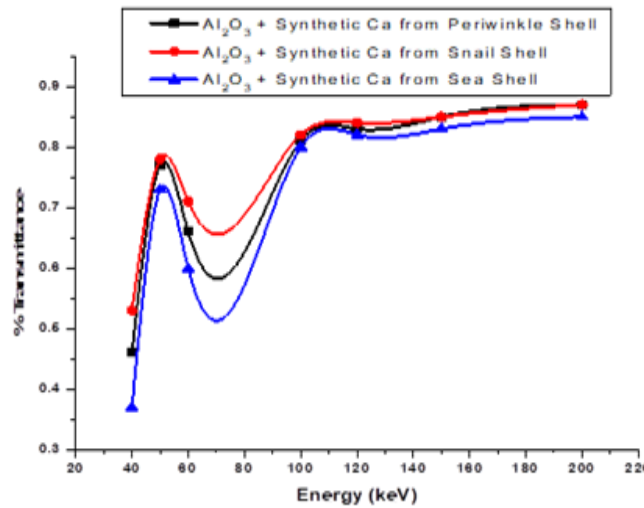


Fig. 7 - % Transmittance of x-ray photons against the energy (keV)

The quality of the x-ray beam, the character of the atoms in the material being investigated, as well as the density and thickness of the substance, all influence x-ray absorption. The density of the shadow created on the radiograph is determined by the quantity of x-ray absorption by the substance. Ca-Al₂O₃ polymer-based composites with high calcium content derived from seashells have the highest absorbance values at the energies under investigation. The absorbance of the Periwinkle shells and Snail shells calcium sources radiation shielding composites varied as well, with Periwinkle calcium source having greater values at 60 keV and below but being comparable at 150 keV and 200 keV. The three composites had absorbance values ranging from 2.075 to 2.43 a.u.

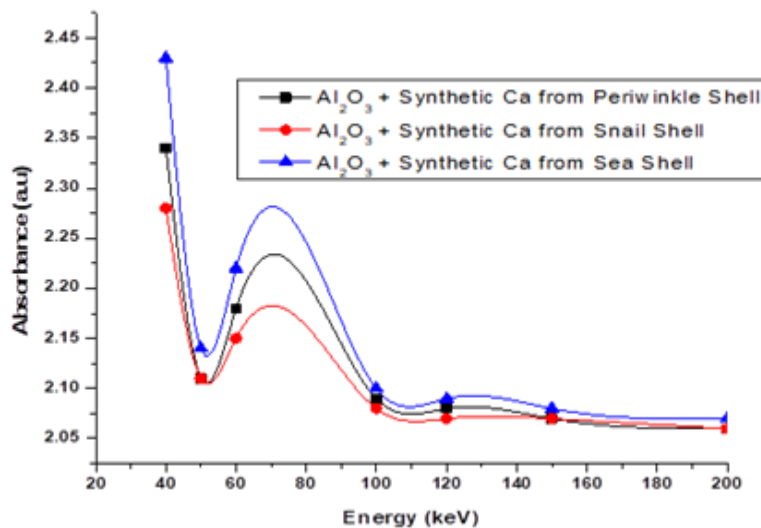


Fig. 8 - Absorbance of x-ray photons against the energy (keV)

At all x-ray energies studied, the measured values of linear attenuation coefficient rose with increasing calcium concentration in all radiation shielding composites. For Ca-Al₂O₃ polymer-based composites with calcium contents sourced from seashells, Periwinkle shells, and Snail shells, the maximum linear attenuation coefficients were 1.0 cm⁻¹, 0.79 cm⁻¹, and 0.65 cm⁻¹, respectively. At 60 keV and below, the radiation shielding composites have the highest attenuation coefficient, making them most useful at lower energies.

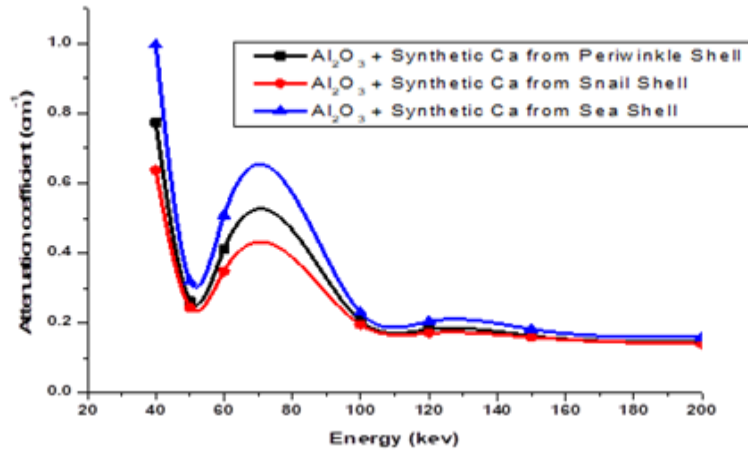


Fig. 9 - Linear attenuation coefficient against energy for the composites

The half-value layer (HVL) is the thickness of attenuating material required to reduce an x-ray's kerma to half its original value, and it offers crucial information about the radiation's energy properties. For a particular x-ray beam, a low half-value layer implies that the x-ray beam has more low energy and less penetrating radiation strength. The HVLs of the produced radiation shielding composites behave differently at different energies of the x-ray beams radiation, as seen in Fig. 10. At 40 and 60 keV, the HVL of all the samples under investigation declined abruptly, then increased linearly as the energy increased from 100 to 200 keV. This offers the thicknesses of the produced composites that must be utilized to attenuate x-ray radiation to half of its original value at different energies.

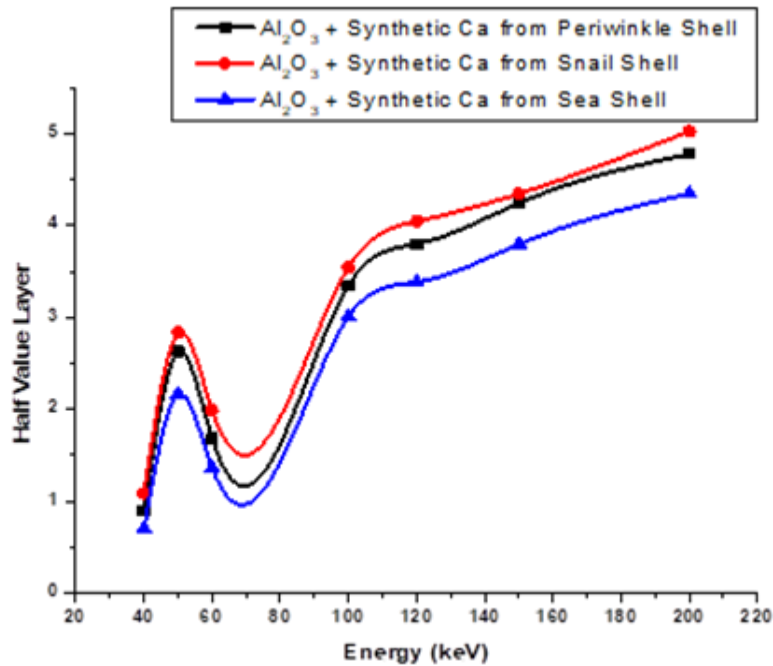


Fig. 10 - Relationship between HVL and energy (keV)

The relaxation length (λ) is determined using the linear attenuation coefficient (μ) of all samples in the energy range 40 keV-200 keV, and it varies with photon energy as shown in Fig. 11. The average distance between two successive contacts is represented by the relaxation length (λ) of any given radiation. The shorter a material's relaxation length is at a given energy, the better its shielding qualities are. The relaxation length (λ) is mathematically similar to the reciprocal of the linear attenuation coefficient (μ). In comparison to other x-ray sources employed at higher energy,

the relaxation length is relatively short at 40 keV and 60 keV, as shown in this plot. This indicates that the radiation shielding composites will cause x-ray photons to lose energy over a short distance for low-energy sources and a relatively long distance for high-energy sources.

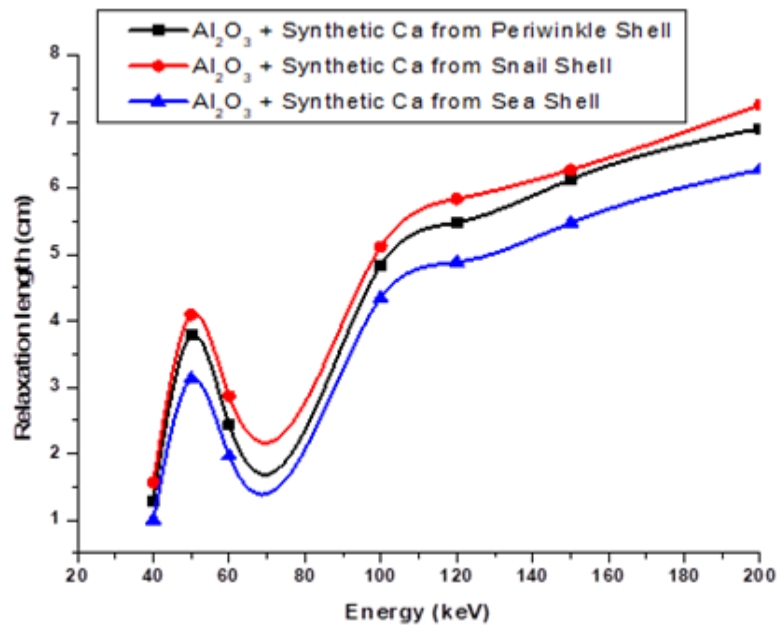


Fig. 11 - Relaxation length against energy (keV)

4. Conclusion

The fabricated low-cost radiation shielding composites of 1 cm thickness demonstrated varying attenuating capacities at different energy used. Ca-Al₂O₃ polymer-based radiation shielding composites with relatively higher calcium contents sourced from seashells had higher x-ray attenuating characteristics than other composites over a specific photon energy range (40 keV-200 keV). Previous research has proved that at energy of an irradiation 59 keV, materials with contemporary thickness in this work are sufficient for protection. At higher energy of irradiation, higher thicknesses of composites are required. The attenuating capacities of these composites can be enhanced upon by increasing the thicknesses of the radiation shielding composites.

Acknowledgement

The authors acknowledge the materials science group, Department of Physics, University of Ilorin.

References

- [1] Wang, B., Ting, C. Y., Lai, C. S., & Tsai, Y. S. (2021). Bismuth Pelvic X-Ray Shielding Reduces Radiation Dose Exposure in Pediatric Radiography. *BioMed Research International*, 2021, 1-7.
- [2] Lee, M. C., Lloyd, J., & Solomito, M. J. (2017). Poor utility of gonadal shielding for pediatric pelvic radiographs. *Orthopedics*, 40(4), e623-e627.
- [3] Chan, C. T. P., & Fung, K. K. L. (2015). Dose optimization in pelvic radiography by air gap method on CR and DR systems—A phantom study. *Radiography*, 21(3), 214-223.
- [4] Karami, V., Zabihzadeh, M., Shams, N., & Gholami, M. (2017). Radioprotection to the gonads in pediatric pelvic radiography: effectiveness of developed bismuth shield. *Int J Pediatr*, 5(6).
- [5] Karami, V., Zabihzadeh, M., & Shams, N. (2018). Bismuth radioprotective gonadal shields: prevalence of use and effect on image quality during paediatric pelvic radiography. *Hong Kong Journal of Radiology*, 21(3), 178-183.
- [6] Davies, B. H., Manning-Stanley, A. S., Hughes, V. J., & Ward, A. J. (2020). The impact of gonad shielding in anteroposterior (AP) pelvis projections in an adult: a phantom study utilising digital radiography (DR). *Radiography*, 26(3), 240-247.
- [7] Li, Z., Zhou, W., Zhang, X., Gao, Y., & Guo, S. (2021). High-efficiency, flexibility and lead-free X-ray shielding multilayered polymer composites: layered structure design and shielding mechanism. *Scientific reports*, 11(1), 4384.

- [8] Mirzaei, M., Zarrebini, M., Shirani, A., Shanbeh, M., & Borhani, S. (2019). X-ray shielding by a novel garment woven with melt-spun monofilament weft yarn containing lead and tiny particles. *Textile Research Journal*, 89(1), 63-75.
- [9] Kalkornsuranee, E., Intom, S., Lehman, N., Johns, J., Kothan, S., Sengloyluan, K., ... & Kaewkhao, J. (2022). Mechanical and gamma radiation shielding properties of natural rubber composites: effects of bismuth oxide (Bi₂O₃) and lead oxide (PbO). *Materials Research Innovations*, 26(1), 8-15.
- [10] Abdel-Aziz, M. M., Badran, A. S., Abdel-Hakem, A. A., Helaly, F. M., & Moustafa, A. B. (1991). Styrene-butadiene rubber/lead oxide composites as gamma radiation shields. *Journal of Applied Polymer Science*, 42(4), 1073-1080.
- [11] Binu, P. P., George, K. E., & Vinod-Kumar, M. N. (2014). Preparation, mechanical and thermal characterization of isophthalic polyester/cloisite 15a nanocomposite. *Int. J. Des. Manuf. Technol.* 5, 148–154.
- [12] Dubey, K. A., Chaudhari, C. V., Suman, S. K., Raje, N., Mondal, R. K., Grover, V., ... & Varshney, L. (2016). Synthesis of flexible polymeric shielding materials for soft gamma rays: Physicomechanical and attenuation characteristics of radiation crosslinked polydimethylsiloxane/Bi₂O₃ composites. *Polymer Composites*, 37(3), 756-762.
- [13] Mirzaei, M., Zarrebini, M., Shirani, A., Shanbeh, M., & Borhani, S. (2019). X-ray shielding behavior of garment woven with melt-spun polypropylene monofilament. *Powder Technology*, 345, 15-25.
- [14] Nambiar, S., Osei, E. K., & Yeow, J. T. (2013). Polymer nanocomposite-based shielding against diagnostic X-rays. *Journal of Applied Polymer Science*, 127(6), 4939-4946.
- [15] El-Fiki, S., El Kameesy, S. U., Nashar, D. E., Abou-Leila, M. A., El-Mansy, M. K., & Ahmed, M. (2015). Influence of bismuth contents on mechanical and gamma ray attenuation properties of silicone rubber composite. *Int. J. Adv. Res.* 3(6), 1035-1041.
- [16] Nambiar, S., & Yeow, J. T. (2012). Polymer-composite materials for radiation protection. *ACS Applied Materials & Interfaces*, 4(11), 5717-5726.
- [17] Harish, V., Nagaiah, N., Prabhu, T. N., & Varughese, K. T. (2009). Preparation and characterization of lead monoxide filled unsaturated polyester based polymer composites for gamma radiation shielding applications. *Journal of Applied Polymer Science*, 112(3), 1503-1508.
- [18] Fan, W. C., Drumm, C. R., Roeske, S. B., & Scrivner, G. J. (1996). Shielding considerations for satellite microelectronics. *IEEE Transactions on Nuclear Science*, 43(6), 2790-2796.
- [19] Hemalatha, K. S., Rukmani, K., Suriyamurthy, N., & Nagabhushana, B. M. (2014). Synthesis, characterization and optical properties of hybrid PVA-ZnO nanocomposite: a composition dependent study. *Materials Research Bulletin*, 51, 438-446.
- [20] Verdipoor, K., Alemi, A., & Mesbahi, A. (2018). Photon mass attenuation coefficients of a silicon resin loaded with WO₃, PbO, and Bi₂O₃ micro and nano-particles for radiation shielding. *Radiation Physics and Chemistry*, 147, 85-90.
- [21] Park, S., Kim, H., Kim, Y., Kim, E., & Seo, Y. (2018). Multilayer-structured non-lead metal/polymer composites for enhanced X-ray shielding. *MRS Advances*, 3(31), 1789-1797.
- [22] Hosseini, S. H., Askari, M., & Ezzati, S. N. (2014). X-ray attenuating nanocomposite based on polyaniline using Pb nanoparticles. *Synthetic Metals*, 196, 68-75.
- [23] Martinez, L. M., & Kingston, J. (2012). Space radiation analysis: Radiation effects and particle interaction outside the earth's magnetosphere using GRAS and GEANT4. *Acta Astronautica*, 72, 156-164.
- [24] Sonsilphong, A., & Wongkasem, N. (2014). Light-weight radiation protection by non-lead materials in X-ray regimes. *2014 International Conference on Electromagnetics in Advanced Applications (ICEAA)*. pp. 656-658.
- [25] Salawu, M. A., Gbolahan, J. A., & Alabi, A. B. (2021). Assessment of Radiation Shielding Properties of Polymer-Lead (II) Oxide Composites. *Journal of the Nigerian Society of Physical Sciences*, 423-428.
- [26] Kim, H., Lim, J., Kim, J., Lee, J., & Seo, Y. (2020). Multilayer Structuring of Nonlead Metal (BiSn)/Polymer/Tungsten Composites for Enhanced γ -Ray Shielding. *Advanced Engineering Materials*, 22(6), 1901448.
- [27] Korkut, T., Gencel, O., Kam, E., & Brostow, W. (2013). X-ray, gamma, and neutron radiation tests on epoxy-ferrochromium slag composites by experiments and Monte Carlo simulations. *International Journal of Polymer Analysis and Characterization*, 18(3), 224-231.
- [28] Udagani, C., & Seshadri, B. S. (2012). Study of gamma attenuation characteristics of high density polyethylene. *International Journal of Science Research*, 1(2), 68-71.
- [29] Sallam, O. I., Alhodaib, A., Abd El Aal, S., & Ezz-Eldin, F. M. (2021). Influence of gamma ray on optical and structural properties of commercial glass enriched with copper oxide. *Inorganic Chemistry Communications*, 124, 108388.
- [30] La, L. B., Leatherday, C., Leong, Y. K., Watts, H. P., & Zhang, L. C. (2018). Green lightweight lead-free Gd₂O₃/epoxy nanocomposites with outstanding X-ray attenuation performance. *Composites Science and Technology*, 163, 89-95.

- [31] Azman, N. N., Siddiqui, S. A., Hart, R., & Low, I. M. (2013). Effect of particle size, filler loadings and x-ray tube voltage on the transmitted x-ray transmission in tungsten oxide—epoxy composites. *Applied Radiation and Isotopes*, 71(1), 62-67.
- [32] Kim, Y., Park, S., & Seo, Y. (2015). Enhanced X-ray shielding ability of polymer–nonleaded metal composites by multilayer structuring. *Industrial & Engineering Chemistry Research*, 54(22), 5968-5973.
- [33] Alabi, A. B., Salawu, M. A., Jimoh, R. A., Akomolafe, T., & Oluwayemi, M. (2020). Appraisal of mechanical properties of different particle sizes of palm kernel shell, coconut shell and mixed palm kernel-coconut shells particles epoxy-filled composites. *Sri Lankan Journal of Physics*, 21, 1-10.
- [34] Saheed, Y. O., Salawu, M. A., & Alabi, A. B. (2022). Mechanical Evaluation and Minerals Phases Identification of Fine and Coarse Okelele Block Clay Composites for Furnace Lining Application. *Journal of the Nigerian Society of Physical Sciences*, 27-33.
- [35] Farahmandjou, M., & Golabiyan, N. (2019). Synthesis and characterisation of Al₂O₃ nanoparticles as catalyst prepared by polymer co-precipitation method. *Materials Engineering Research*, 1(2), 40-44.
- [36] Ma, M. G., Zhu, Y. J., & Xu, Z. L. (2007). A new route to the synthesis of -alumina nano-rods. *Materials Letters*, 61(8-9): 1812- 1815.
- [37] Dahiru, D., Yusuf, U. S., & Paul, N. J. (2018). Characteristics of concrete produced with periwinkle and palm kernel shells as aggregates. *FUTY Journal of the Environment*, 12(1), 42-61.
- [38] Ogunipe, K. E., Ogunbayo, B. F., Olofinnade, O. M., Amusan, L. M., & Aigbavboa, C. O. (2021). Affordable housing issue: Experimental investigation on properties of eco-friendly lightweight concrete produced from incorporating periwinkle and palm kernel shells. *Results in Engineering*, 9, 100193.
- [39] Ezike, S. C., Hyelnasinyi, C. N., Salawu, M. A., Wansah, J. F., Ossai, A. N., & Agu, N. N. (2021). Synergistic effect of chlorophyll and anthocyanin Co-sensitizers in TiO₂-based dye-sensitized solar cells. *Surfaces and Interfaces*, 22, 100882.
- [40] Ajayi, A. A., Alabi, A. B., Abodunrin, O. W., Akinsola, I. S., Olawole, O. C., Salawu, M. A., & Ayeni, A. (2021). Influence of solvents on properties of ZnS thin films synthesized by chemical spray pyrolysis technique. *Jordan Journal of Physics*, 14(4), 346-357.
- [41] Salawu, M. A., Alabi, A. B., Adeleke, J. T., Sulu, H. T., Sharafa, S. B., & Akomolafe, T. (2019). Effects of Temperature on Morphological, Structural and Optical Characteristics of CdTe Films for PV Applications. *Nigerian Journal of Basic and Applied Sciences*, 27(1), 10-16.
- [42] Salawu, M. A., Alabi, A. B., & Sharafa, S. B. (2018). Optical Properties of Chemically Synthesized Cadmium Sulphide for Solar Cell Applications. *Jordan Journal of Physics*, 11(3), 201-207.
- [43] Salawu, M. A., Alabi, A. B., Akomolafe, T., & Omoniyi, F. O. (2019). Effects of Annealing Temperature on Optical and Electrical Conductivity of (80 nm ITO)/(100 nm ZnO) Transparent Conducting Oxide Multilayer. *Physics Memoir-Journal of Theoretical & Applied Physics*, 1(1), 31-37.
- [44] Salawu, M. A., Alabi, A. B., & Akomolafe, T. (2018). Effects of post deposition thermal treatments on 80 nm ito ultra-thin film substrates for optoelectronics applications. *FUOYE International Journal of Pure and Applied Sciences*, 3(1), 155- 166.
- [45] Salawu, M. A., Ayobami, A. A., Adebisi, A., Ezike, S. C., Saheed, Y. O., & Alabi, A. B. (2022). Characterization of eosin red and hibiscus sabdariffa-based dye-sensitized solar cells. *Optical Materials*, 127, 112177.